Modeling growth from the vapor and thermal annealing on micro- and nanopatterned substrates

Marcos F. Castez and Roberto C. Salvarezza
Instituto de Investigaciones Fisicoquímicas Teóricas y Aplicadas (INIFTA), UNLP, CONICET, Casilla de Correo 16, Sucursal 4, (1900) La Plata, Argentina

Hernán G. Solari
Departamento de Física, Facultad de Ciencias Exactas y Naturales, Universidad de Buenos Aires, Pabellón I, Ciudad Universitaria, (1428) Buenos Aires, Argentina

(Received 2 September 2005; revised manuscript received 14 December 2005; published 27 January 2006)

We propose a (1+1)-dimensional mesoscopic model to describe the most relevant physical processes that take place while depositing and/or annealing micro- and nanopatterned solid substrates. The model assumes that a collimated incident beam impinges over the growing substrate; scattering effects in the vapor and reemission processes are introduced in a phenomenological way as an isotropic flow. Surface diffusion is included as the main relaxation process at the micro- or nanoscale. The stochastic model is built following population dynamics considerations; both stochastic simulations and the deterministic limit are analyzed. Numerical aspects regarding its implementation are also discussed. We study the shape-preserving growth mode, the coupling between shadowing effects and random fluctuations, and the spatial structure of noises using numerical simulations. We report important deviations from linear theories of surface diffusion when the interfaces are not compatible with the small slope approximation, including spontaneous formation of overhangs and nonexponential decay of pattern amplitudes. We discuss the dependence of stationary states with respect to the boundary conditions imposed on the system.

DOI: 10.1103/PhysRevE.73.011607 PACS number(s): 81.10.Bk, 02.50.Ey, 81.15.Aa, 81.16.−c

I. INTRODUCTION

In the last years a large amount of theoretical and experimental work has been done in the field of interface dynamics. The central motivation for these efforts has been mainly related to producing high quality deposited films for different technological applications.

Theoretical work has been performed with different aims and tools. There are at least three different perspectives clearly identified: (A) cellular automata discrete models [1,2]; (B) stochastic differential equations (SDEs) [3–6]; (C) multiscale modeling [7]. The theoretical work differs not only in the methods and assumptions but also in aims.

Theoretical work of types A and B has focused in developing discrete and continuous models that can describe interface evolution for different growth processes such as vapor deposition, sputtering, chemical vapor deposition, molecular beam epitaxy, electrodeposition, and sedimentation, while much of the experimental work has been mainly conceived to verify the validity of those models. Most of these works have been done under the framework of dynamic scaling concepts [8,9]. Using this approach different growth models in the time-asymptotic limit have been grouped into "universality classes" in order to understand the physical processes (surface diffusion, evaporation-condensation, the presence of concentration or pressure fields) that control interface properties (and film quality). Growth models and experiments have mainly been made for deposition on planar smooth substrates, and in most cases, under the assumption of growing interfaces with small slopes and without holes and overhangs.

The rapid development of technology toward miniaturization, particularly nanotechnology, has opened a new scenario for the study of interface dynamics involving nanostructured substrates with different shapes (and aspect ratios) and the deposition of small amounts of material. These two facts lead to important differences with respect to traditional work in this field: (1) the small slope approximation could be no longer valid; (2) crossover regimes become important because the system is far from the asymptotic limit [10]. Here the central problem is to control the shape of the deposited layer during the growth process. In fact, in many cases it could be important to reproduce the shape of the nanostructured substrate in the deposited film (self-preserving growth) while in others it could be important to modify it in a controlled way (for instance by changing temperature [11] or deposition rate) the initial shape leading to different architectures. Recent comparison of SDE models with experimental results [12] concerning patterned surfaces of technologically relevant thickness have shown that, despite the number of free parameters available, these models fail to capture essential features of the dynamics.

The modeling of technologically relevant situations has received far less attention than universality classes. New models are expected to have the following properties.

(1) The ability to deal with patterned surfaces with any slope, and multivaluated surfaces.

(2) Incorporation of measurable constants, such as surface diffusion rates.

(3) Inclusion of the different processes in independent form (models of type A present no diffusion in the absence of deposition, for example), thus being useful in multistep processes.

(4) Mesoscopic models should also incorporate stochasticity specific of the physical processes, rather than the external noise considered in type B.

(5) The link with the physical processes should be explicit so that failure of the model can be traced back to inappropriate physical hypotheses.

Within this perspective, only the multiscale model [7] is, to our knowledge, compatible with this program. Additionally, we also expect the formulation to be sufficiently simple and compact to allow for some global (theoretical) understanding beyond simulations.

In this context, in this paper we introduce a model especially concerned with the study of two of the most important physical processes that take place while depositing and annealing over micro- and nanostructured materials. The model is constructed from geometrical and physical considerations, as well as basic population dynamics, i.e., stochastic processes of discrete events.

Concerning deposition processes, we discuss the shape-preserving growth mode, the spatial structure of noise and the coupling between shadowing effects and fluctuations. With respect to annealing processes over micro- and nanostructured substrates, we found, away from the small slope approximation, interesting deviations from predictions of linear surface diffusion theory, including a spontaneous generation of overhangs and nonexponential decay of pattern amplitudes. Finally, we discuss the approach to the stationary state in the asymptotic limit, and the role of the boundary conditions imposed on the system.

The rest of this paper is organized as follows. In Sec. II we discuss the basic physics of the model; numerical issues are discussed in Sec. III; in Sec. IV we present analytical results for some limit cases of the model; in Secs. V and VI we present numerical results on the processes of deposition and thermal treatments, respectively. Finally, Sec. VII presents a summary and concluding remarks.

II. DEFINITION OF THE MODEL

A. Physical processes relevant to the description

In this section we discuss the physical motivation of the model. Let us consider a substrate immersed into a vapor at a certain pressure, while a collimated beam of particles is directed to the substrate, from an arbitrary incidence direction. Molecules from the incident beam may collide against the background vapor molecules. We assume that molecules in the vapor are chemically inert with respect to the molecules in the beam and in the substrate.

When a particle from the incident beam impacts onto the substrate, it may get stuck on it (inelastic process), or it may be reemitted (elastic process). The probabilities associated with these events depend on the energy of the incident particles, the substrate temperature, the chemical nature of the involved species, the local crystalline structure in the impact region, etc. Nevertheless, in this work we do not attempt to solve this complicated quantum-mechanical problem, and we mask all these effects under a phenomenological parameter: the sticking coefficient S, which represents the probability that the collision of a particle from the incident beam with the substrate to be inelastic. Therefore, $1-S$ will be the reemission probability.

We elaborated a $(1+1)$-dimensional model for two reasons: In the first place, we do not want to obscure understanding due to an overloaded notation, and secondly, because many systems in which our model could be useful have translational invariance in one direction, and thus the relevant system is really $1+1$ dimensional. However, most of our results and conclusions can be extended to the $(2+1)$-dimensional case.

Let us consider an interface element ΔS: particles that travel ballistically through the vapor with no scattering event impinge on it, and, therefore, they have a well-defined incidence direction. These particles form what we shall call *directed flow*. Moreover, some of the particles that impact onto ΔS may come from random directions after experiencing one or more scattering processes (through collisions with vapor molecules or scattering due to reemission [13,14]). These particles form what we shall call *random flow*.

At the submicrometer scale, the most important transport process is surface diffusion (evaporation-condensation processes dominate at a larger scale). Among the most important simplifications imposed on the model, we can mention the following: the model does not include bulk diffusion effects, nor internal stress fields. Moreover, no crystalline properties are taken into account; thus it is expected that the model could be applied to amorphous solids and polycrystalline solids with a relatively small grain size.

B. Stochastic evolution of the interface

Let us consider again a surface element ΔS in the interface (described by a smooth curve on the plane), small enough to be approximately contained in the tangent line at a certain point $\vec{P}$ in ΔS. Let $\vec{n}$ be the unitary outward normal vector to the curve at $\vec{P}$ and let $\vec{d}$ be the unitary vector directed along the incidence direction, but in the opposite sense. Thus, the directed flow can be written as $-J_d\vec{d}$, where J_d is the number of particles that cross a transversal element per length and time units. In the same way, the isotropic flow can be characterized by J_i. We assume that the overall substrate is small as compared with the scales at which flows change, or, equivalently, we assume that J_d and J_i are constant over the complete interface.

The number of particles in the directed beam that impacts on the element ΔS contains a factor of cross section [15] $\cos\gamma$, where γ is the angle between $\vec{n}$ and $\vec{d}$. Thus, the number of particles aggregated onto element ΔS by inelastic collisions in a time dt is

$$N_{dep} = (\mathcal{S}_d J_d \cos\gamma\epsilon + \mathcal{S}_i J_i)\Delta S\, dt, \tag{1}$$

where $\mathcal{S}_d$ and $\mathcal{S}_i$ are the sticking coefficients of the directed and isotropic beams, respectively, while ϵ is a function that takes into account the eventual geometrical shadowing [16–18] of the directed flow by other parts of the interface (therefore, ϵ will be a nonlocal function, depending on the complete interface). Much writing is saved by introducing the growth rate in the absence of shadowing

$$F = (\mathcal{S}_d J_d + \mathcal{S}_i J_i)\sigma, \tag{2}$$

where σ is the average size of the particles in the flow, and the fraction of random flow p is defined through the relationship

$$p = \frac{\mathcal{S}_i J_i}{\mathcal{S}_d J_d + \mathcal{S}_i J_i}. \tag{3}$$

It is a well-established fact that the surface diffusion current is proportional to the gradient of chemical potential μ, and that this is proportional to the local interface curvature $\mathcal{C}$ [8,11,19–21]. The number of particles that come in (or leave) the element ΔS by surface diffusion is (by a direct application of the Green's theorem), at the first order in ΔS,

$$N_{dif} = -\frac{K}{\sigma}\frac{\partial^2 \mathcal{C}}{\partial s^2}\Delta S\, dt, \tag{4}$$

where K is proportional to the surface diffusion coefficient [11,21], and s is the arc length parameter.

Evidently, N_{dep} and N_{dif} are stochastic variables. In this sense, we consider that Eqs. (1) and (4) provide the average of these stochastic quantities. We observe that the most relevant contribution to the fluctuations come from the Poisson process representing the arrival of particles approaching at a constant rate to the surface. Following firmly established knowledge in population dynamics [22–25] and considering that only the arrival of a very large number of small particles will modify the surface, the noise terms of the deposition and diffusion processes respond to spatially uncorrelated stochastic variables with variance equal to the flow arriving to the surface element. This means that there are certain coefficients C_{dep} and C_{dif} so that

$$|\delta N_{dep}| = C_{dep}\sqrt{N_{dep}} \tag{5}$$

and

$$|\delta N_{dif}| = C_{dif}\sqrt{\frac{2K}{\sigma}\left|\frac{\partial \mathcal{C}}{\partial s}\right| dt}. \tag{6}$$

We take $C_{dep}=C_{dif}=1$ in almost all cases, although this coefficients will be useful in Sec. VI D to "switch off" the noise by putting $C_{dep}=C_{dif}=0$.

Further notice that Eqs. (5) and (6) correspond to the fluctuation of the number of particles arrived at the surface element ΔS. The deterministic limit consists then in allowing the particle size to decrease to zero while the number of particles goes to infinity and the product of both quantities (the layer thickness) is kept finite.

III. NUMERICAL IMPLEMENTATION

We assume that the interface between the growing solid and the vapor can be described at time t by a smooth parametric curve

$$\vec{r}(s,t) = (r_x(s,t), r_y(s,t)) \tag{7}$$

where s is the arc length parameter. We take the x and y axes parallel and perpendicular to the substrate baseline, respectively. To reduce border effects, we impose periodic boundary conditions to the system. Other boundary conditions are considered in Sec. VI D, when we discuss the long time limit of annealing processes.

We take N points $\vec{P}_i$ $(i=1,2,\ldots,N)$ sampled from the curve. Each pair of consecutive points defines a segment S_i. The periodic boundary conditions identify the point to the right of the Nth point with the point $\vec{P}_1$; therefore we have N segments that conform to a piecewise linear function that is close to the original interface in the usual sense of calculus.

In the previous section we showed how we obtain the number of particles "incoming" or "outgoing" from a given piece of interface ΔS due to the random and directed flows and to surface diffusion. If $\mathcal{N}$ particles of size σ get stuck onto the segment S_i of length ΔS_i, this segment will be translated a distance $U_i^{(S)}(s)=\mathcal{N}\sigma/\Delta S_i$ following the local outward normal to the interface. Computing the quantities $U_i^{(S)}$ for each segment, it is clear that we can update the complete interface by moving each segment in this way. Nevertheless, as $U_i^{(S)}$ are stochastic quantities, an update of this kind would result in the loss of continuity of the piecewise linear function, or conversely, it would be necessary to add new segments "on the fly" as the interface evolves, to preserve the continuity of the function. Thus, we found the first difficulty in the implementation of the model: physically it is convenient to consider how segments have to be updated, but from a computational perspective, such a procedure is very unsuitable, since to get a continuous interface new degrees of freedom must be added, which leads to a rapid consumption of the computational resources.

From a computational point of view, it is much more convenient to build an algorithm so that the updating is made over points rather than over segments: updating N points we obtain N points that define N segments, then the points and segments numbers are conserved over the complete evolution.

To translate the computed segments update into points update, immediately two alternatives emerge: Either we constrain the volume [or, more precisely, the area in our $(1+1)$-dimensional model] to be conserved in each segment or we make an average among neighboring segments. The first option constitutes a nonlocal algorithm, in which all segments are coupled. The second option results in a local algorithm. We have compared the performance of both algorithms: while they coincide in terms of the interface mean, the nonlocal algorithm introduces a fictitious high frequency noise (the nonlocal algorithm violates the "causality law"), being, thus, inappropriate to describe fluctuations. Therefore, we only consider in this work the local algorithm, in which point updates are obtained through the following relationship of conservation of the average volume:

$$U_i^{(P,N)} = \frac{U_i^{(S)}\Delta S_i + U_{i-1}^{(S)}\Delta S_{i-1}}{\Delta S_i + \Delta S_{i-1}}. \tag{8}$$

We have indicated that the evolution of the interface proceeds in the direction of the local normal to the curve, a rule that is based on symmetry arguments. Nevertheless, to be rigorous, we have $2N$ variables [N vectors of two compo-

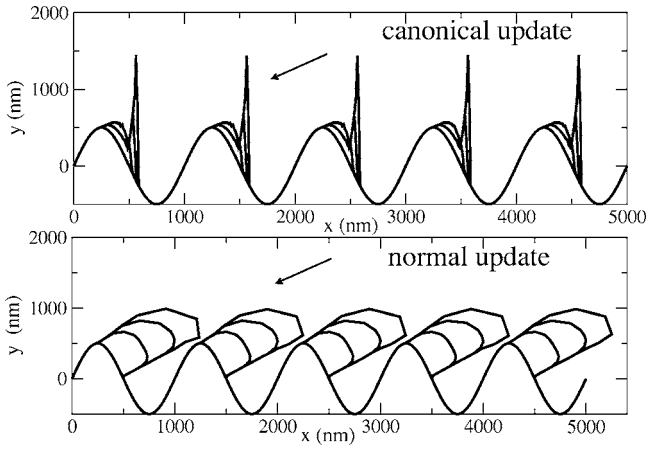

FIG. 1. Above: Artifacts produced by the canonical update strategy in situations where the evolution generates overhangs. Below: Proper evolution with the normal update. Simulations correspond to a pure directed flow in the direction indicated by the arrows. Parameter values were $F=2$, $p=0$, $\theta=50°$, $T=600$, $\sigma=0.1$, $C_{dep}=C_{dif}=1$, and the total elapsed time was 400.

nents (r_x, r_y)] and only N constraints (8). Thus we can choose freely the direction of the update vector. While the normal direction is the proper update direction in most cases due to symmetry reasons, there are situations in which other update strategies may be preferred. For example, when the initial interface can be described as a single-valued function $f(x)$, an update in the direction of the y axis is convenient, since distances between neighboring points remain bounded from below. This fact prevents the algorithm from running into numerical instabilities that occur when points become too close. In this sense, this update strategy leads to a more stable algorithm than the normal direction update. For the sake of brevity, we shall refer to the two update strategies as "canonical" and "normal" updates.

For the canonical update, Eq. (8) becomes

$$U_i^{(P,C)} = \frac{U_i^{(S)}\Delta S_i + U_{i-1}^{(S)}\Delta S_{i-1}}{2dx}, \tag{9}$$

where dx is the distance between the abscissas of neighboring points.

It is important to notice that the canonical update has an important limitation: it can only deal with single-valued interfaces. Interfaces can be multivalued (i.e., they can have overhangs) from the beginning of the process and overhangs can also appear spontaneously in an initially single-valued interface because of its own evolution. Therefore, in situations in which an overhang development is expected, the canonical update produces artifacts in the evolution (see Fig. 1), and the normal update must be used.

In summary, in situations where there is no overhang development we can use the canonical update which is generally more stable (of course when both strategies are applicable, both will produce the same physical predictions, since they are two implementations of the same model). However, in those situations in which we must deal with multivalued interfaces, only the normal update is acceptable.

IV. FUNDAMENTAL DIFFERENCE EQUATION AND ITS DETERMINISTIC LIMIT

After having discussed the physical aspects of the model and their implementation issues, we can put all the information together in an equation that summarizes the model (in the normal update approach):

$$\vec{U}_i^{(S)}(t \to t+dt) = \left[\left(Fp + F(1-p)\cos(\gamma)\epsilon - K\frac{\partial^2 \mathcal{C}}{\partial s^2} \right) dt + \sqrt{[Fp + F(1-p)\cos(\gamma)\epsilon]\frac{\sigma dt}{\Delta S_i}}\,\eta + \sqrt{\frac{2K\sigma}{(\Delta S_i)^2}\left|\frac{\partial \mathcal{C}}{\partial s}\right| dt}\,\xi \right] \vec{n}, \tag{10}$$

where γ is the angle between the local normal $\vec{n}$ and the vector $\vec{d}=(\sin\theta, \cos\theta)$, θ is the angle between the normal to the substrate and $\vec{d}$ measured in a clockwise fashion, while η and ξ are independent random variables, with mean equal to 0 and variance equal to 1.

Equation (10) is a stochastic, state-dependent, vectorial equation that provides a general framework for modeling film solid growth from vapor deposition in the presence of surface diffusion. Contrarily to the usual assumption in the literature [8,9,26] of state-independent noise, in Eq. (10) noise terms depend on the state, i.e., noise depends on the properties (local and nonlocal) of the interface.

Equation (10) will be investigated in depth in the following sections by means of Monte Carlo simulations. Nevertheless, before moving into the simulations, it is interesting to study the deterministic limit, obtained in the "unphysical" limit when the particle size $\sigma \to 0$:

$$\frac{\partial \vec{r}(s,t)}{\partial t} = \left(Fp + F(1-p)\cos(\gamma)\epsilon - K\frac{\partial^2 \mathcal{C}}{\partial s^2} \right)\vec{n}. \tag{11}$$

Equation (11) is a continuous "underlying" equation for the model, since it does not contain any reference to the discretization "steps" ΔS_i. It is interesting to analyze in some detail a few particular cases of Eq. (11).

When $p=0$ (we have only directed flow), Eq. (11) shows different behaviors depending on whether the geometrical shadowing is or is not important, i.e., depending on the shape of the interface and on the incidence angle θ. If shadowing is important, the areas of interface exposed to the flow will grow, while the shadowed regions will not. For instance, if we have a sinusoidal wave with an aspect ratio large enough so that shadowing takes place under oblique incidence, the peak-valley distance will increase continuously, i.e., growth is unstable.

When there is no shadowing (i.e., $\epsilon=1$ over the complete interface) and when there are no overhangs, it is convenient to describe the interface as a single-valued function $y(x)$. In this way, the vectorial evolution can be replaced by a simpler scalar evolution. In fact, let $\alpha(x)$ be the angle between the local normal $\vec{n}$ and the normal to the substrate, measured in a clockwise fashion. It is evident that

$$\frac{\partial y(x,t)}{\partial x} = -\tan[\alpha(x,t)] \tag{12}$$

while the no-overhang condition implies that $-\pi/2 < \alpha(x,t) < \pi/2 \ \forall (x,t)$. By elementary geometrical considerations it can be shown that a point in the interface updated through $\vec{U}_i^{(S)}(t \to t+dt) = U_i^{(S)}(t \to t+dt)\vec{n}$ leads to incrementing $y(x)$ by Δy, according to

$$\Delta y = \frac{U_i^{(S)}(t \to t+dt)}{\cos(\alpha)}. \tag{13}$$

Thus, when shadowing and overhangs are absent, Eq. (11) has a scalar "counterpart"

$$\frac{\partial y(x,t)}{\partial t} = \frac{Fp + F(1-p)\cos(\gamma) - K\partial^2 \mathcal{C}/\partial s^2}{\cos(\alpha)}. \tag{14}$$

Equation (14) is nonlinear (mainly due to the term $\partial^2 \mathcal{C}/\partial s^2$) and we did not attempt to find a full solution to it. On the other hand, we analyzed a few particular cases that, nevertheless, are very important to understand many of the most remarkable aspects of the evolution. For instance, when there is no diffusion ($K=0$) the resulting equation is

$$\frac{\partial y(x,t)}{\partial t} = \frac{Fp + F(1-p)\cos(\alpha - \theta)}{\cos(\alpha)}, \tag{15}$$

where we have used that $\cos(\gamma) = \cos(\theta - \alpha)$. For a pure directed flow ($p=0$), we have

$$\frac{\partial y(x,t)}{\partial t} = F\cos(\theta) - F\sin(\theta)\frac{\partial y(x,t)}{\partial x}. \tag{16}$$

The solution to the first-order linear partial differential equation if the initial interface is described by a function $y_0(x)$ is [27]

$$y(x,t) = F\cos(\theta)t + y_0[x - F\sin(\theta)t], \tag{17}$$

which means that the initial interface just performs a rigid translation in the direction of vector $\vec{d}$; this translation property is the origin of the shape-preservation growth phenomenon, which we shall discuss in Sec. V A. When the flow is purely isotropic ($p=1$), Eq. (15) turns into

$$\frac{\partial y}{\partial t} = \frac{F}{\cos(\alpha)} = F(1 + y'^2)^{1/2}. \tag{18}$$

Under the hypothesis of small slopes ($y' \ll 1$) and expanding to the first nontrivial contribution $(1+y'^2)^{1/2} \sim 1 + \frac{1}{2}y'^2$ we obtain the deterministic part of the well-known (diffusionless) Kardar-Parisi-Zhang (KPZ) equation [3]. Then by varying the fraction p of isotropic flow, Eq. (15) bridges between a KPZ-like evolution (18) and a shape-invariant evolution (17). As is well known, KPZ-like evolution destroys the patterns (fills the cavities due to lateral growth) after a certain deposited thickness.

Under the small slope approximation, we can get an approximate solution in the presence of surface diffusion ($K \neq 0$) for pure directed flow ($p=0$), generalizing in this way the result given by Eq. (17). In fact, under this assumption, the "complicated" term $\partial^2 \mathcal{C}/\partial s^2$ gets linearized $\partial^2 \mathcal{C}/\partial s^2 \sim \partial^4 y/\partial x^4$, and Eq. (14) becomes

$$\frac{\partial y(x,t)}{\partial t} = F\cos(\theta) - F\sin(\theta)\frac{\partial y(x,t)}{\partial x} - K\frac{\partial^4 y}{\partial x^4}. \tag{19}$$

By a direct substitution into Eq. (19) we can see that a Fourier mode of the initial interface $A\sin(kx)$ evolves at time t into

$$Ft\cos(\theta) + A\exp(-Kk^4 t)\sin\{k[x - Ft\sin(\theta)]\}. \tag{20}$$

Equation (20) is an interesting result since it shows that every Fourier mode performs a rigid translation in the direction of vector $\vec{d}$, coupled with an exponential decay whose lifetime depends on temperature through the constant K and on the wavelength λ, which is proportional to λ^4.

It is important to stress that Eq. (20) was obtained in the deterministic limit and in the small slope approximation. In Sec. VI A we show the persistence of this result in the presence of noise, while in Sec. VI B we show how interesting deviations take place when situations far from the small slope approximation are considered.

V. NUMERICAL SIMULATIONS OF DEPOSITION PROCESSES

In this section we begin to expose results from numerical simulations of model. We have included the temperature in simulations through the dependence of the surface diffusion coefficient with temperature reported in [11] for copper. The values of temperature must be translated into values of the surface diffusion coefficient to apply our results to noncopper deposits. Unless other explicit indications are made to the contrary, in this work we report distances in nanometers, times in seconds, and temperatures in kelvins.

A. Shape-invariant growth and shadowing effects

An interesting phenomenon is that of shape-invariant growth. Equation (20) indicates that, in the deterministic limit, for pure directed flow the interface performs a rigid translation coupled with a frequency-dependent decay by surface diffusion. In terms of the complete equation, Fig. 2 shows an example of shape invariant growth.

Even in cases where initially no shadowing is expected, shadowing effects can become important due to their coupling with fluctuations. In this way, fluctuations originated by deposition noise can be amplified by shadowing effects, resulting in the development of large-scale instabilities. This kind of instability can be suppressed by carrying out the deposition at higher temperatures, since temperature-activated surface diffusion filters high frequency fluctuations. These effects are illustrated in Fig. 3, where shadowing-fluctuation coupling promotes the triggering of instabilities when the growth is made at 300 K, while no instability appears when the deposition process is made at 500 K.

Summarizing, to obtain shape-invariant growth the following conditions must be observed.

(1) Random flow must be suppressed as much as possible, for example, by reducing the pressure in the deposition

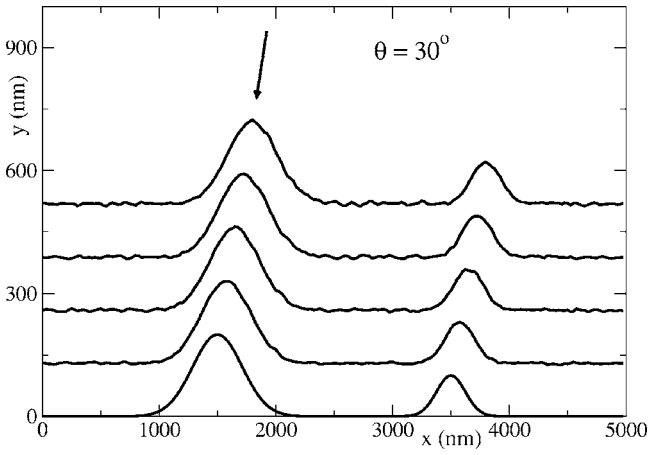

FIG. 2. Shape-invariant growth, obtained for a pure directed beam with a direction indicated by the arrow. Parameter values were $F=1$, $p=0$, $\theta=30°$, $T=400$, $\sigma=1$, $C_{dep}=C_{dif}=1$, and the total elapsed time was 600.

chamber to assure a large mean free path for the particles in the incident beam.

(2) The initial geometry of the substrate and the incidence angle must be such that shadowing effects are not important.

(3) Deposition rates must be small enough to constrain fluctuations below a certain threshold.

(4) Temperature must be large enough to constrain the fluctuations at values below those in which shadowing begins to be relevant, but must be small enough to avoid an important decay of the high frequencies of the interfaces.

Thus, to obtain the necessary conditions to get shape-invariant growth, a careful analysis of substrate geometry, temperature ranges, chemical nature of deposit, pressure ranges, etc., must be made, which explains why the shape-invariant growth is not so easy to obtain [28–30].

Experimental results showing shape-invariant growth on a patterned Cu substrate and comparison with model simulations have been presented in [31]. Shape-invariant growth

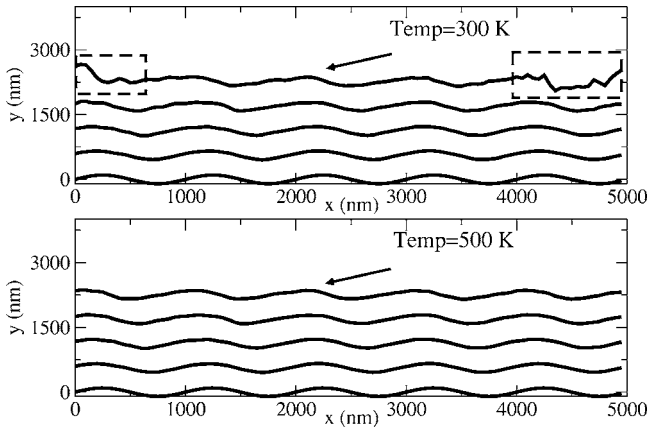

FIG. 3. Above: Triggering of instabilities (stressed with dashed boxes) by fluctuation-shadowing coupling at low temperatures (300 K). Below: No instabilities occur at 500 K. The rest of the parameters are $F=10$, $p=0$, $\theta=60°$, $\sigma=1$, $C_{dep}=C_{dif}=1$, and the total elapsed time was 450.

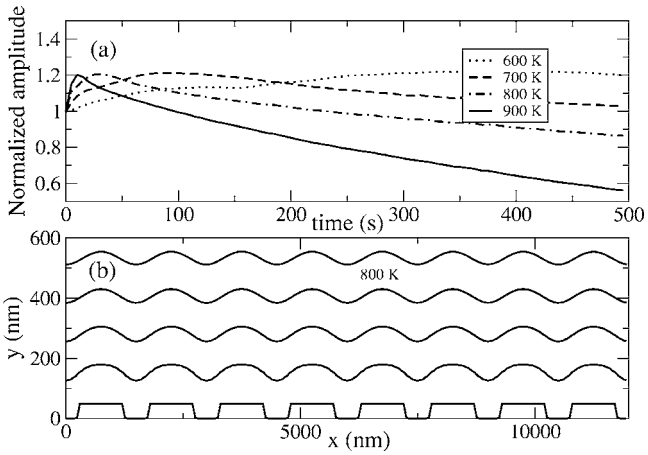

FIG. 4. Surface growth for slab pattern ($B_i=500$ $B_s=1000$). (a) Corrugation (normalized amplitude) versus time at four different temperatures. (b) Evolution of the deposited pattern.

and the triggering of instabilities by the interaction between shadowing and random fluctuations was illustrated showing good agreement between simulations and experiments.

B. Lateral growth of patterned surfaces

Direct flow promotes growth preserving the surface shape. In contrast, isotropic aggregation is associated with cavity filling and an eventual decrease of the corrugation (understood as the height difference between the highest peak and the most profound valley).

Experimental results [12] indicate that the change in corrugation measured during deposition in a bidimensional setup, created as an array of cylindrical pits, is not monotonic in time and depends on the distance between pits as well as the pit widths. In [12] the authors report an increase in corrugation at the early stages and a decrease at later times.

Although the present model cannot reproduce bidimensional surfaces, it is fair to ask whether there is indication of the observed behavior within the present model or, in the opposite case, whether it fails in the same terms as KPZ models.

To explore the question we set up a surface consisting of smoothed rectangular patterns and changed the separation between slab and slab width in the range 300–700 nm for a copper substrate at 700 K (an arbitrarily chosen temperature), studying the growth of the material depositing up to an average of 500 nm of material.

The results are summarized in Figs. 4 and 5. In Fig. 4 we show the dependence of the corrugation on the growth time (roughly speaking, the average deposition) for several temperatures for the process. In all cases the corrugation presents a maximum that moves to higher times with decreasing temperatures. In the lower part of the figure we present some profiles at different stages of the growth process.

In Fig. 5 we present results of growth at 700 K for different initial conditions. B_i stands for the interslab distance and B_s for the slab width. In all cases there is an initial increase of the corrugation followed by a decrease. The maximum

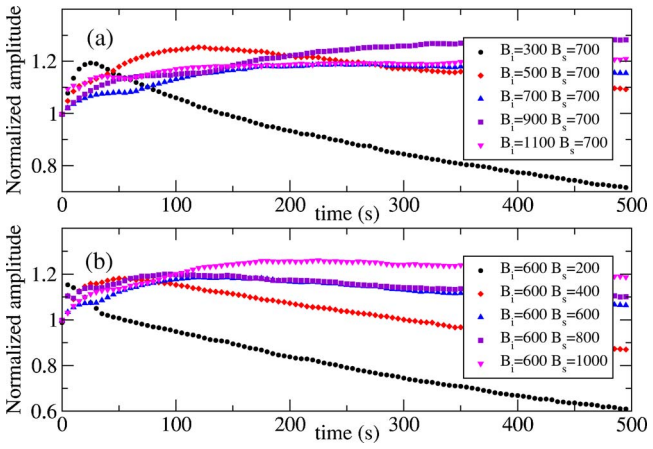

FIG. 5. (Color online) Corrugation (normalized amplitude) versus time for varying (slab) initial conditions. (a) Constant slab width. (b) Constant inter slab distance.

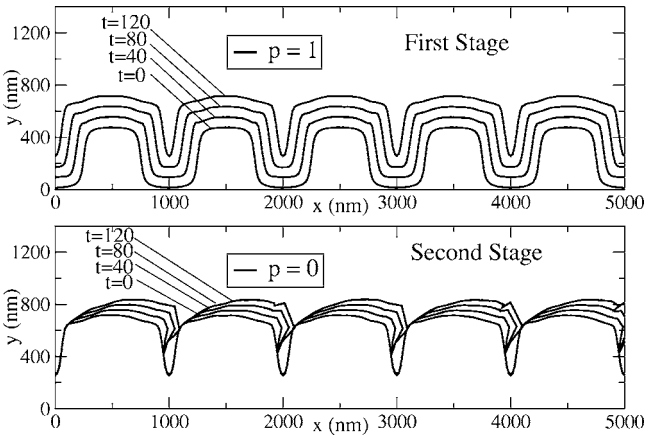

FIG. 6. Development of a periodic array of nanocavities of controlled size, by combining 120 s of isotropic deposition (above) with 120 s of directed deposition (below) to $\theta=60°$. The rest of parameters were $F=2$, $T=500$, $\sigma=1$, and $C_{dep}=C_{dif}=1$.

corrugation as well as the deposition time corresponding to it depend on B_i as well as on B_s.

The corrugation presents an initial increase with the deposition process, reaches a maximum, and then decreases, showing the same qualitative dependence as the experiment and contrasting with the KPZ solutions. The location and amplitude of the maximum corrugation depend on slab width, interslab distance, and temperature and are of the order of magnitude reported in the experiments.

Results from Figs. 4 and 5 are in good qualitative agreement with observations in recent experiments on homoepitaxial growth on a patterned GaAs(001) substrate [12], although a more quantitative comparison is not suitable since in these experiments there are important processes, such as crystalline asymmetry and island nucleation, that have no place in our model.

C. Hybrid deposition processes

So far, we have been focusing on "one-stage" processes, in which all parameters remain fixed from the beginning to the end of the process; it is evident that it would be interesting to consider the possibility of complementing the characteristics of a growth mode obtained for certain sets of parameters with the characteristics obtained with other sets, i.e., to consider a "hybrid" or "multistage" approach.

Multistage methods are common in materials engineering; in fact, it is not hard to find, in micro- and nanotechnology, recipes to build materials with specific properties, having several tens of stages, each one requiring a specific control of the intervening variables [32].

There is a very broad range of possible combinations of growth modes, and all deserve a careful consideration as to the feasibility of their implementation in the laboratory. We shall not attempt a detailed description of the possible combinations of methods, and we shall limit ourselves to considering just one example.

Figure 6 (above) shows simulations of growth after 120 s of a pure isotropic deposition ($p=1$) on a patterned substrate. The isotropic flow is used to modify (increase) the aspect ratio of the pattern. Then we made a deposit over another 120 s with a totally directed flow ($p=0$) under an incidence angle $\theta=60°$, as is shown in Fig. 6 (below). In this case we used increased aspect ratio and shadowing effect to get closed cavities. In this way we obtained a periodic array of size-controlled nanocavities.

D. Spatial structure of noise

Up to now, we have discussed results concerned mainly with the deterministic aspects of the model. The stochastic nature of the evolution was only revealed through a noise on the deterministic evolution. Only in the case in which noise-promoted fluctuations were coupled with shadowing effects, as was discussed in Sec. V A, stochasticity plays a fundamental role, since the generated instabilities drastically changed the subsequent evolution.

In this section we shall consider other predictions of the model concerned with the spatial structure of noise. This originates from the fact that Eq. (10) has multiplicative factors that depend on the interface topography, i.e., they depend on the state, contrarily to the way in which noise is introduced in most models in the literature [8,9].

Concerning the noise related to the deposition process, dependence on topography is due to the dependence on the angle between the local normal and the incidence direction. This dependence is associated with a physical prediction: the noise due to directed flow must be more important at regions where the incidence is quasinormal. This prediction is verified by means of simulations, as it is shown in Fig. 7, where a pure directed beam impinges vertically ($\theta=0$) on a patterned substrate. It can be seem that regions in the interface normal to the incidence direction are much noisier than regions where the incidence is quasitangential.

Of course, isotropic flow is also isotropic concerning the noise that it promotes; therefore noise associated with isotropic flow is spatially homogeneous over the complete interface.

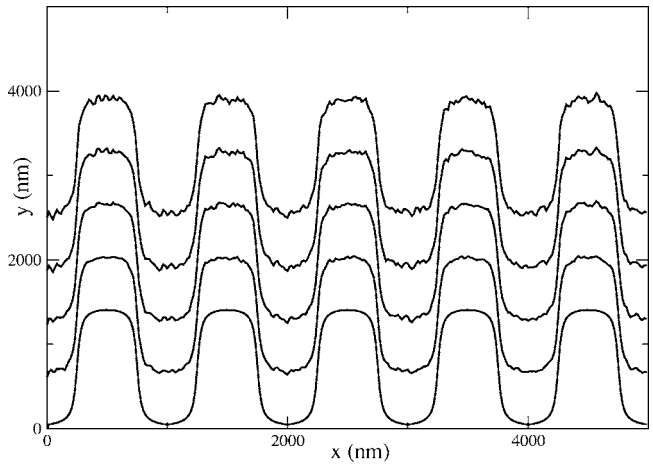

FIG. 7. Spatial structure of noise developed when a pure directed flow ($p=0$) impinges on a patterned substrate. The growth was achieved in 500 s at 300 K with $F=5$ and under normal incidence ($\theta=0$). The rest of the parameters were $C_{dep}=3.16$, $C_{dif}=1$, and $\sigma=1$.

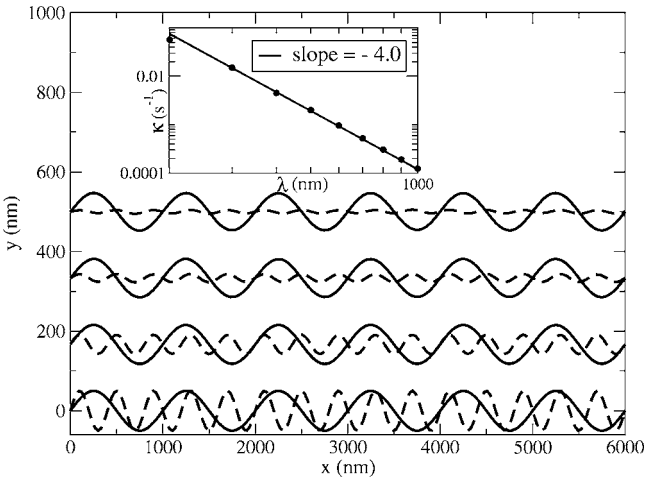

FIG. 8. Decay of small aspect ratio sinusoidal interfaces. Inset: log-log plot of the decaying constant as a function of the wavelength λ. Parameter values were $F=1$, $p=0$, $\theta=0°$, $T=600$ K, $\sigma=0.1$, $C_{dep}=C_{dif}=1$, and total time elapsed was 500 s.

VI. NUMERICAL SIMULATIONS OF THERMAL TREATMENTS

We shall now study the case of null incoming flow ($F=0$). Thus, the only operative process is surface diffusion, while the temperature is the main control parameter. No particles are added to the substrate, then this case can be physically interpreted as the performing of a thermal treatment of the substrate. The study of the decaying of structures by surface diffusion is important since it is intrinsically related to the morphological stability of nanostructures [33].

A. Decay of sinusoidal patterns under the small slope approximation

From numerical simulations performed starting with sinusoidal patterns satisfying the small slope approximation, we have obtained results entirely consistent with those from the deterministic limit for small slopes, indicated in Eq. (20), and, in consequence, these are in complete agreement with linear models for surface diffusion, which are well studied in the literature, in which surface diffusion is associated with a term proportional to $\nabla^4 h$ in a linear Langevin equation for the height h [2,34]. In particular, Fig. 8 shows the dependence of the decay velocity on the wavelength of the sine wave. In the inset of Fig. 8 it can be seen that the decay constant κ depends on the wavelength through $\kappa=\lambda^{-4}$, in agreement with linear surface diffusion theory.

B. Decay of sinusoidal patterns far from the small slope approximation

While profiles lying under the small slope approximation evolve according to linear theories of surface diffusion, this is not the case when we consider waves with aspect ratios on the order of unity or larger, as is shown in Fig. 9, where the actual evolution and the solution in the small slope approximation are simultaneously plotted, as given by Eq. (20). As is shown in Fig. 9, the actual evolution for a large aspect ratio wave deviates significantly from predictions of the linear theory of surface diffusion.

Simulation results for the annealing of a sinusoidal profile at 800 K are shown in Fig. 10. In (a) and (b) the profile evolution and the temporal evolution of its amplitude are shown, respectively, for a small amplitude wave. The exponential decay observed is that expected from the linear theory of surface diffusion. However, when the initial profile is a sinusoidal wave with an amplitude large enough to be away from the small slope approximation, we observe a deviation from the exponential amplitude decay [Fig. 10(d)], accompanied by a spontaneous generation of regions where the interface is multivalued [Fig. 10(c)], i.e., the dynamics of surface diffusion itself generates overhangs. This means that, depending on the aspect ratio, the annealing process can also be used not only to modify the physical properties but also to

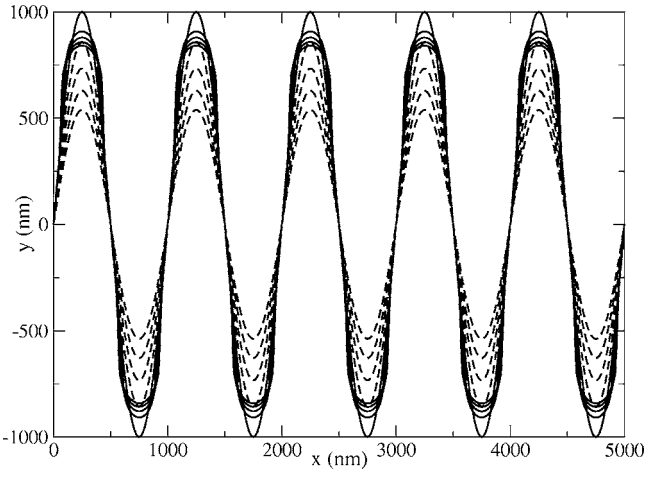

FIG. 9. Comparison between the actual evolution of model (solid lines) and the analytical solution in the small slope approximation (dashed lines) at 500 K. Remaining parameter values were $F=0$, $\sigma=1$, $C_{dif}=1$, and the total elapsed time was 500 000.

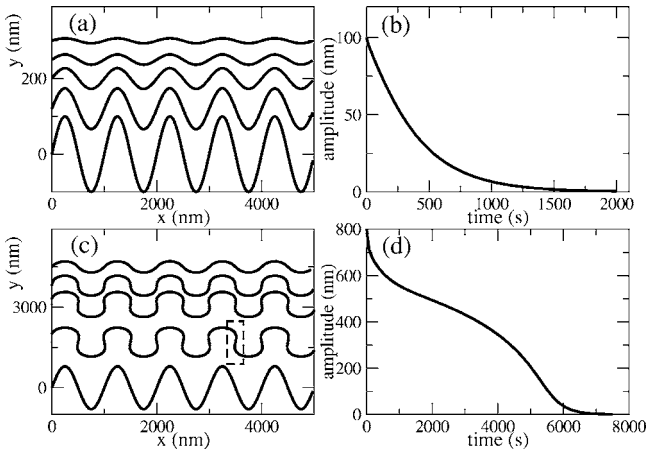

FIG. 10. (a) and (c) Annealing snapshots (at 800 K) for sine waves with initial amplitudes 100 and 800 nm, respectively, and zero incident flow ($F=0$). Curves are offset for clarity (all must have zero mean). Box in (c) stresses the overhang formation. (b) and (d) Wave amplitude time evolutions corresponding to cases (a) and (c), respectively. Remaining parameters were $\sigma=1$ and $C_{dif}=1$.

manipulate the shape of the structured film in postdeposition conditions.

Far from the small slope approximation, the decay in amplitude is exponential for short periods of time as can be observed in Fig. 10(d). In the small slope case, the decay constant was proportional to λ^{-4}. Thus, we proceeded to investigate how this dependence behaves away from the small slope approximation. As shown in the inset of Fig. 11, the decay constant κ (obtained from the first 10 s of the annealing process) follows closely a dependence $\kappa \propto \lambda^{-3.4}$. This dependence is in good agreement with previous results for a discrete model [35], in which an exponent -3.5 ± 0.1 was reported.

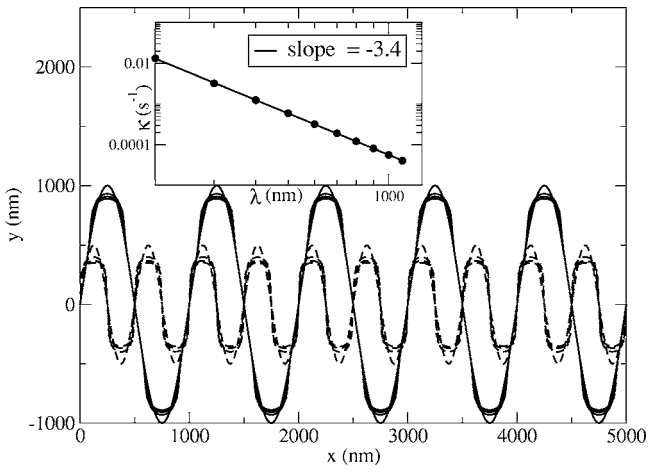

FIG. 11. Decay of large aspect ratio sinusoidal interfaces. Inset: Log-log plot of the decay constant as a function of λ. Parameter values were $F=0$, $T=700$, $\sigma=1$, $C_{dif}=1$, and the total elapsed time was 300.

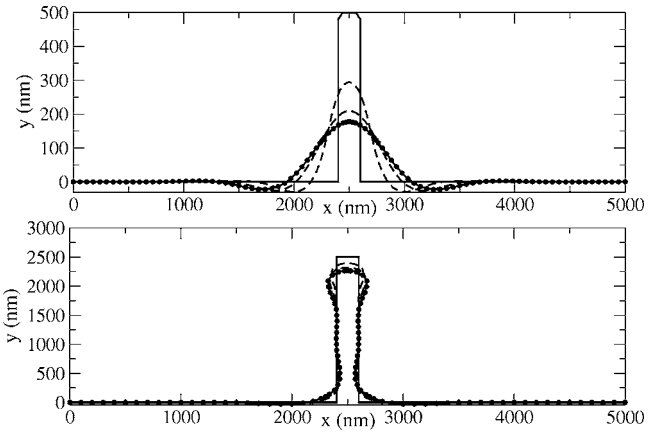

FIG. 12. Decay of rectangular structures with different heights by means of thermal annealing at 700 K, during 3000 s. Remaining parameters were $F=0$, $\sigma=1$, and $C_{dif}=1$.

C. Decay of nonperiodic structures

In this section we consider briefly the annealing of substrates that initially have rectangular aperiodic structures. Structure decay through surface diffusion requires mass transport over the interface; surface diffusion is a thermally activated process; thus (as observed in simulations) a faster decay is expected at larger temperatures.

When rectangular structures are annealed, in the early stages of the process a reduction in the base in conjunction with an enlargement at the top is observed. In consequence, in the same way that occurs when considering large aspect ratio sinusoidal patterns decay, evolution leads to a spontaneous overhang generation. This interesting phenomenon is shown in Fig. 12, where annealing is performed during 3000 s at 700 K over a rectangular structure of 200 nm at the base width and a height of 500 nm (above), and over another structure 200 nm base width and height 2500 nm (below). The described effect can be observed only for the rectangle with larger height (below) as, for the considered times and temperatures, the characteristic diffusion length is larger than the height in the plot above, while this is not the case in the plot below, thus permitting distinguishing these scales. To see the effect for the geometry of the plot above it is necessary to observe the process with a finer time scale.

D. Stationary states and the role of boundary conditions

In the preceding sections we have focused on the study of interface evolution when the substrate was exposed to a thermal treatment during a *finite* time. This means that we have studied the initial stages of the surface diffusion relaxation process. In this section we shall consider the long time behavior, i.e., we shall be looking for the equilibrium state to which the interface approaches after a thermal treatment for a time $t\to\infty$. Although the consideration of this limit can be useful in certain applications, this subject has an intrinsic importance from a theoretical point of view.

We have shown in Sec. VI B that a sinusoidal profile with a moderately large aspect-ratio is distorted, at the initial stage, into a multivalued interface. If we now suppose that

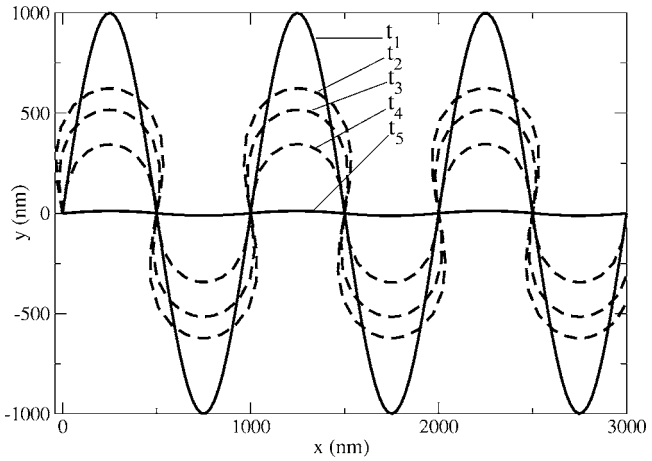

FIG. 13. Approach to equilibrium of a profile initially sinusoidal. Parameter values were $F=0$, $T=800$, $\sigma=1$, $C_{dif}=1$, and the total elapsed time was 10 000.

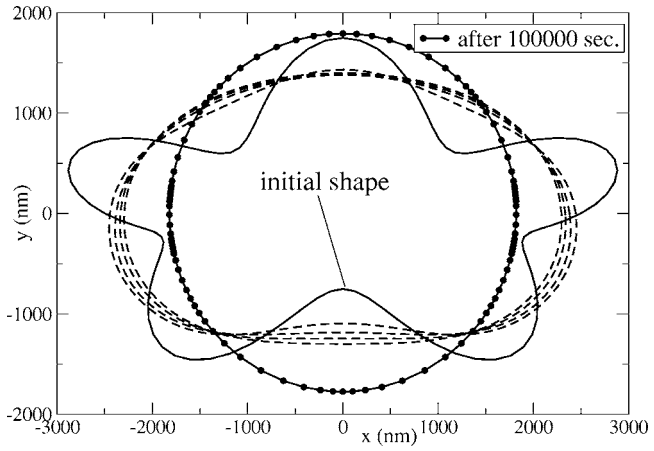

FIG. 14. Evolution of an arbitrary shape onto a stationary state with circular shape. Parameter values were $F=0$, $T=1200$, $\sigma=1$, and $C_{dif}=1$.

we continue with the thermal annealing during a very long time, what will the final, equilibrium shape of the interface be? Why? Figure 13 answers the first question: The final state is a flat interface. Providing an answer to the second question is the aim of the following discussion.

The stationary state requires that the flow of particles by surface diffusion should remain constant over the complete interface, or equivalently, that the second derivative of the local curvature with respect to the arc length parameter be zero:

$$\frac{\partial^2 \mathcal{C}}{\partial s^2} = 0. \tag{21}$$

From Eq. (21) it can be concluded that the possible stationary states are in the two-parameter family of linear functions:

$$\mathcal{C}(s) = As + B. \tag{22}$$

The fact that we have imposed periodic boundary conditions on the system requires that, $\forall t$, the curvature should remain identical at the edges, implying that $A=0$ in Eq. (22), i.e., the curvature in the stationary state, must be constant along the complete interface. It is easy to see that the only smooth and periodic curves with constant curvature are in the family of horizontal straight lines $y=cte$, where the constant is determined by the initial condition, due to the conservative character of surface diffusion.

To obtain stationary states different to the one described above we must explore other boundary conditions. For example, we can consider *natural* boundary conditions, in which the edges are closed over themselves, with which interface turns into a closed curve embedded in a plane. In this case, the boundary condition implies again that the curvature in the stationary state must be constant. As is well known, a plane, smooth, and closed curve with constant curvature must be a circumference. The radius of this circumference must be such that the area of the circle coincides with the area enclosed by the initial interface, again because of the conservative nature of surface diffusion. This result can be clearly observed in Fig. 14, which shows how a closed curve with an arbitrary initial shape evolves into a circumference.

The periodic and natural boundary conditions impose that $A=0$ in the linear general solution (22). To obtain stationary states where the curvature does not remain constant, it is necessary to consider a boundary condition in which edges are free, i.e., where edges are unconnected. We assume that the curvatures at the edges are kept equal to certain constants, i.e., we fix the value of the curvature at the first (point 1) and at the last (point N) points in the curve: $\mathcal{C}[1]=\mathcal{C}_1$ and $\mathcal{C}[N]=\mathcal{C}_N$.

In this case the stationary state is effectively a curve whose curvature is proportional to the arc length. That is precisely the main characteristic of the curve known as a *Cornu spiral* [36], a curve that finds many applications in diverse topics such as diffraction theory in optics [37] and expressway junctions in urban planning [38]. The Cornu spiral is defined as a parametric curve $\vec{e}(t)=(S(t),C(t))$, where $S(t)$ and $C(t)$ are the sine and cosine Fresnel integrals, respectively [39]. The Cornu spiral is shown in Fig. 15.

The stationary state for free boundaries is a segment of the Cornu spiral. The approach to the stationary state is shown in Fig. 16, where it can be seen that the interface gets asymptotically close to a segment of the Cornu spiral, while the curvature assumes a linear dependence on arc length.

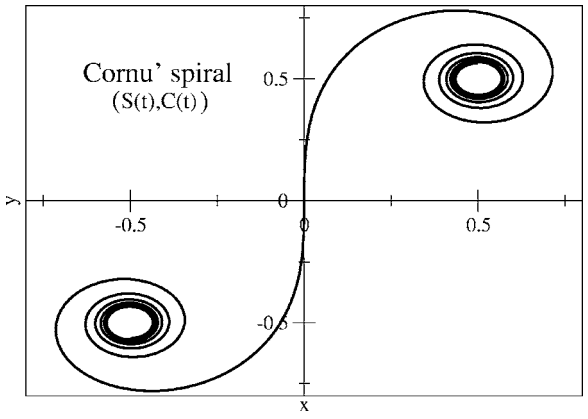

FIG. 15. The Cornu spiral.

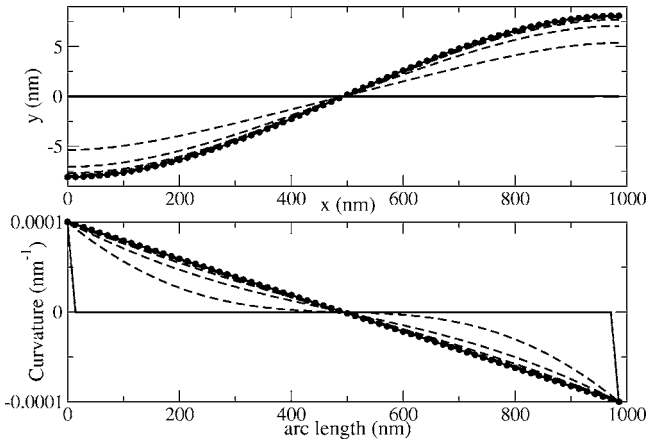

FIG. 16. Above: Approximation of the interface to a stationary state that is a piece of the Cornu spiral for free boundary conditions. Below: Dependence of curvature on arc length when the interface approaches the stationary state. Parameter values were $F=0$, $T=950$, $C_{dif}=0$.

The position of the center and spatial orientation of the Cornu spiral that contains the stationary state interface depends on initial conditions, as can be seen in Fig. 18, in which the evolution is followed for several initial conditions, showing how the stationary state has roughly the same shape irrespective of the initial conditions, although the final placement and orientation of the curve differ from case to case.

It is interesting to note that in the cases of periodic and natural boundary conditions, the stationary state is established even in the presence of diffusive noise, while the stationary states obtained for free boundaries, shown in Figs. 16 and 17, were obtained by switching off the diffusive noise (i.e., fixing $C_{dif}=0$). In fact, when the stretch of diffusive noise is increased, the system moves away from the stationary state, as is shown in Fig. 18.

Based on exhaustive numerical simulations, we can conclude that, for free boundaries, no stationary state is established when diffusive noise is present. We may say that, for periodic and natural boundary conditions, stationary states

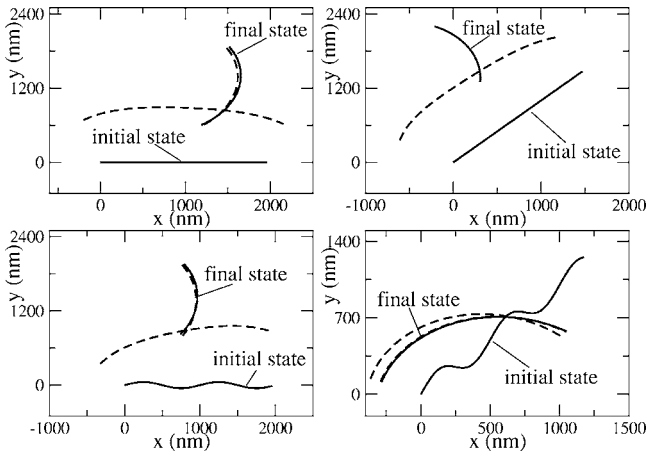

FIG. 17. Approach to the stationary state under several initial conditions under free boundary conditions. Parameter values were $F=0$, $T=1000$, $C_{dif}=0$, $\mathcal{C}_1=-0.0012$, and $\mathcal{C}_N=0.001$.

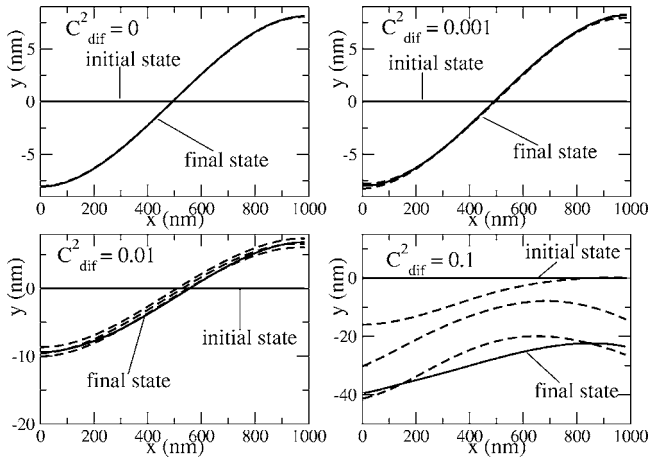

FIG. 18. Evolution of the interface for large times in the free boundaries case, for several intensities of the diffusive noise coefficient C_{dif}. Remaining parameters were $F=0$, $T=950$, $\sigma=1$, and the total elapsed time was 5000.

are robust to noise, while the stationary state for a free boundary condition is not robust to noise. This fact can be easily understood, if we remember that diffusive noise is proportional to $\sqrt{\partial\mathcal{C}/\partial s}$. For natural and periodic boundary conditions, the stationary state has a constant curvature, therefore $\partial\mathcal{C}/\partial s=0$, producing then a noise-free stationary state. For free boundaries, the derivative of curvature is constant along the complete interface; therefore diffusive noise is always present, leaving no room for the formation of a stationary state.

VII. SUMMARY

In this work we have introduced a $(1+1)$-dimensional interface growth model, including deposition of particles (under directed and isotropic incidences) and surface diffusion processes at a mesoscopic scale. We provided a vectorial description of the surface suitable to study the evolution of patterned interfaces, even far from the small slope approximation. Our treatment differs from most of the earlier studies in the literature in several ways: our introduction of the governing equations is based on explicit considerations of physical, geometrical, and statistical nature and as such, the limit of validity is evident. The random fluctuations arise naturally, are directly dictated by the nature of the process, and are not an arbitrary decision of the authors.

Analytical results are reported in the deterministic limit, showing how the shape-preserving growth mode takes place, and the nature of the surface diffusion filtering properties in the small slope approximation. Extensive Monte Carlo simulation results are presented in several (highly nonlinear) cases where no analytical results are available.

Simulations of deposition processes showed several interesting effects such as the coupling between fluctuations and shadowing effects, the spatial structure of noise, and the usefulness of hybrid methods for shape modification. Model predictions are in good qualitative agreement with experiments on depositing Cu over nanopatterned Cu substrates

[31] and are compatible with experiments on homoepitaxial growth over patterned GaAs(001) [12].

Monte Carlo simulations on thermal treatments for interfaces satisfying the small slopes approximation are in complete agreement with the predictions from the linear theory of surface diffusion. Nevertheless, in the general case, simulations show nonexponential decaying modes and spontaneous overhang generation (of course, this cannot be seen using the usual scalar approach).

Finally, we have studied the approach to the stationary state by surface diffusion. We have shown how the shape of this stationary state depends strongly on the boundary conditions imposed on the system. While for periodic and natural boundary conditions a stationary state with constant curvature and robust in front of noise is established, when the boundaries are free a stationary state is obtained only in the absence of diffusive noise; the stationary state in this case is a line with a curvature proportional to arc length, i.e., it is a segment of the Cornu spiral.

ACKNOWLEDGMENTS

This work has been performed as part of the Projects No. PICT 02-11111 of FONCYT and No. X-308 of Universidad de Buenos Aires. M.F.C. acknowledges gratefully a grant from Fundación Antorchas.

[1] F. Family, J. Phys. A **19**, L441 (1986).
[2] D. E. Wolf and J.Villain, Europhys. Lett. **13**, 389 (1990).
[3] M. Kardar, G. Parisi, and Y. C. Zhang, Phys. Rev. Lett. **56**, 889 (1986).
[4] T. Sun, H. Guo, and M. Grant, Phys. Rev. A **40**, R6763 (1989).
[5] Z. W. Lai and S. Das Sarma, Phys. Rev. Lett. **66**, 2348 (1991).
[6] M. D. Johnson, C. Orme, A. W. Hunt, D. Graff, J. Sudijono, L. M. Sander, and B. G. Orr, Phys. Rev. Lett. **72**, 116 (1994).
[7] F. H. Baumann, D. L. Chopp, T. D. de la Rubia, G. H. Gilmer, J. E. Greene, H. Huang, S. Kodambaka, P. O'Sullivan, and I. Petrov, MRS Bull. **26** (3), 182 (2001).
[8] A. L. Barabasi and H. E. Stanley, *Fractal Concepts in Surface Growth* (Cambridge University Press, Cambridge, U.K., 1995).
[9] P. Meakin, *Fractals, Scaling and Growth far from Equilibrium* (Cambridge University Press, Cambridge, U.K., 1998).
[10] M. F. Castez, B. Blum, R. C. Salvarezza, and H. G. Solari, Phys. Rev. E **67**, 061605 (2003).
[11] G. Andreasen, P. L. Schilardi, O. Azzaroni, and R. C. Salvarezza, Langmuir **18**, 10430 (2002).
[12] H. C. Kan, S. Shah, T. T. Tadyyon-Eslami, and R. J. Phaneuf, Phys. Rev. Lett. **92**, 146101 (2004).
[13] J. T. Drotar, Y. P. Zhao, T. M. Lu, and G. C. Wang, Phys. Rev. B **64**, 125411 (2001).
[14] A. K. Chattopadhyay, Phys. Rev. B **65**, 041405(R) (2002).
[15] G. S. Bales and A. Zangwill, Phys. Rev. Lett. **63**, 692 (1989).
[16] R. P. U. Karunasiri, R. Bruinsma, and J. Rudnick, Phys. Rev. Lett. **62**, 788 (1989).
[17] C. Roland and H. Guo, Phys. Rev. Lett. **66**, 2104 (1991).
[18] J. T. Drotar, Y. P. Zhao, T. M. Lu, and G. C. Wang, Phys. Rev. B **62**, 2118 (2000).
[19] W. W. Mullins, J. Appl. Phys. **28**, 333 (1957).
[20] W. W. Mullins, J. Appl. Phys. **30**, 77 (1959).
[21] J. Lapujoulade, Surf. Sci. Rep. **20**, 191 (1994).
[22] S. N. Ethier and T. G. Kurtz, *Markov Processes* (Wiley, New York, 1986).
[23] J. P. Aparicio and H. G. Solari, Phys. Rev. Lett. **86**, 4183 (2001).
[24] H. G. Solari and M. A. Natiello, Phys. Rev. E **67**, 031918 (2003).
[25] H. Solari and M. Natiello, in *Mathematical Modelling in Physics, Engineering and Cognitive Sciences*, edited by A. Khrennikov, Proceedings of the Workshop Dynamical Systems from Number Theory to Probability—2. Vol. 6 (Växjö University Press, Växjö, 2003), pp. 79–94.
[26] P. Meakin, Phys. Rep. **235**, 189 (1993).
[27] I. N. Sneddon, *Elements of Partial Differential Equations* (McGraw-Hill, New York, 1957).
[28] C. S. Torres, *Alternative Lithography: Unleashing the Potentials of Nanotechnology* (Plenum Press, New York, 2004).
[29] C.-S. Son, T. Kim, X.-L. Wang, and M. Ogura, J. Cryst. Growth **221**, 201 (2000).
[30] N. Tsurumachi, C.-S. Son, T. Kim, and M. Ogura, J. Cryst. Growth **237**, 1486 (2002).
[31] M. F. Castez, M. H. Fonticelli, O. Azzaroni, R. C. Salvarezza, and H. G. Solari, Appl. Phys. Lett. **87**, 123104 (2005).
[32] S. M. Rossnagel, J. Vac. Sci. Technol. B **16**, 2585 (1998).
[33] M. V. Ramanamurty, Phys. Rev. B **62**, 17004 (2000).
[34] S. Das Sarma and P. Tamborenea, Phys. Rev. Lett. **66**, 325 (1991).
[35] M. A. Dubson and G. Jeffers, Phys. Rev. B **49**, 8347 (1994).
[36] D. von Seggern, *CRC Standard Curves and Surfaces* (CRC Press, Boca Raton, FL, 1993).
[37] E. Hecht and A. Zajac, *Optics* (Addison-Wesley, Reading, MA, 1974).
[38] A. L. Higgins, *The Transition Spiral* (Van Nostrand, New York, 1922).
[39] *Handbook of Mathematical Functions*, edited by M. Abramowitz and I. A. Stegun (Dover, New York, 1970).